

Learning Stereopsis from Geometric Synthesis for 6D Object Pose Estimation

Jun Wu¹, Lili Liu¹, Yue Wang¹ and Rong Xiong¹ .

Abstract—Current monocular-based 6D object pose estimation methods generally achieve less competitive results than RGBD-based methods, mostly due to the lack of 3D information. To make up this gap, this paper proposes a 3D geometric volume based pose estimation method with a short baseline two-view setting. By constructing a geometric volume in the 3D space, we combine the features from two adjacent images to the same 3D space. Then a network is trained to learn the distribution of the position of object keypoints in the volume, and a robust soft RANSAC solver is deployed to solve the pose in closed form. To balance accuracy and cost, we propose a coarse-to-fine framework to improve the performance in an iterative way. The experiments show that our method outperforms state-of-the-art monocular-based methods, and is robust in different objects and scenes, especially in serious occlusion situations.

I. INTRODUCTION

6D object pose estimation aspires to estimate the rotation and translation of interested objects with regard to certain canonical coordinates. Accurate object pose estimation is the key to many real-world applications, such as robotic manipulation, augmented reality, and human-robot interactions. This is a challenging problem due to the variety of objects appearance, occlusions between objects, and clutter in the scene.

Based on the sensors they adopt, current object pose estimation methods can be roughly categorized into two classes: monocular-based methods [1] [2] [3] and RGBD-based methods [4] [5] [6]. Previous researches have shown that the performance of monocular-based methods are generally less competitive than the other one. Without depth information, monocular-based methods rely greatly on 2D image features to estimate 6D pose, thus involve more uncertainties. Though monocular image lacks 3D awareness in nature, two or more frames of such images combined together implicitly bring out the depth information, as has been verified in many stereo or multi-view stereo tasks [7] [8] [9]. However, when we are not certain about the object pose in one frame, unthinkingly linking another new frame with large baselines might introduce unknowable risks. Thus, we opt to focus on estimating 6D object pose with a *short-baseline two-view* setting, to lower the possibility of bringing more uncertainties.

Intuitively, we consider two pipelines to tackle this problem: *dense-depth* and *sparse-depth*. *Dense-depth* method

aims to recover the dense depth map from two images, then solves the problem following current successful RGBD-based pose estimation methods. But under a short baseline setting, the parallax is probably too small to infer precise depth for all the points. On the other hand, *sparse-depth* method only intends to obtain the depth of sparse keypoints useful for estimating object pose. For example, we can apply monocular-based methods to get 2D keypoints separately from the two images, then triangulate them to 3D space so as to establish the 3D-3D correspondence between scene and model. Nonetheless, this pipeline restores 3D points from two certain 2D points, so is easy to be affected by the uncertainties from either estimation.

Considering these two pipelines, we argue that under a short baseline, restoring only several keypoints is more robust and efficient than recovering the whole 3D scene. But if we restore the sparse keypoint's depth by simply triangulating the already decided 2D keypoints, many precious early learned information is discarded, including semantic information and context information. Therefore, instead of this *sparse-depth late-fusion* pipeline, we attempt to keep as much information as possible to 3D, and directly learn 3D keypoints in geometric space. Therefore, in this paper, we propose a *sparse-depth early-fusion* mechanism to directly learn 3D keypoints by putting the 2D features to their corresponding 3D geometric position, trying to enhance the reliability and accuracy of RGB-based object pose estimation methods.

In summary, the major contributions of this paper are as follows:

- We propose a novel *sparse-depth early-fusion* framework for 6D object pose estimation in a *short-baseline two-view* setting, which constructs a 3D geometric volume to learn the distribution of 3D keypoints, and applies robust solver to estimate the pose.
- We introduce a coarse-to-fine mechanism to predict 3D keypoints from the 3D geometric volume by reducing the divergence between feature field and local keypoint heatmaps.
- We show that our method is robust in different objects and scenes, especially in occlusion scenes, and effectively enhance the estimation accuracy compared to monocular-based methods and our baselines.

II. RELATED WORKS

A. Single-view object pose estimation

Most of the state-of-the-art approaches use single view observation to estimate pose. Some methods take monocular

¹Jun Wu, Lili Liu, Yue Wang and Rong Xiong are with the State Key Laboratory of Industrial Control Technology and Institute of Cyber-Systems and Control, Zhejiang University, Zhejiang, China.

Corresponding author, wangyue@ipc.zju.edu.cn, Co-corresponding author, rxiong@zju.edu.cn

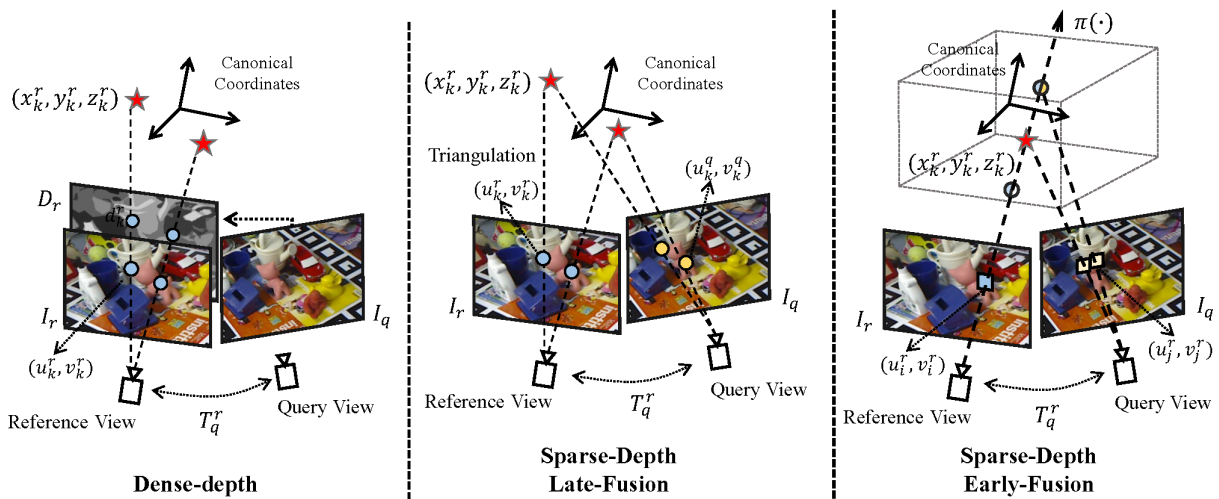


Fig. 1. Illustration of comparing 3 different pipelines to tackle two-view object pose estimation problem. **Left:** Dense-depth. 2D keypoints are computed in the reference view, and a depth map is predicted by reference view and query view images. Together 3D keypoints are predicted. **Middle:** Sparse-depth late-fusion. 2D keypoints are separately predicted in both reference view and query view, then triangulated to 3D space to get 3D keypoints. **Right:** Sparse-depth early-fusion. The images from reference view and query view are combined together to directly predict 3D keypoints.

images as input, and tackle this problem by establishing 2D-3D correspondence, followed by PnP algorithm to solve the pose [2] [10] [11]. Inspired by 2D object detection methods, [12] [13] employs CNN to predict the 3D bounding box corners of the object in the image, and associate the corners with those in 3D CAD models to solve the pose. Since the corners are artificial, the estimation results are not satisfactory. To use more reliable correspondence, PVNet [14] selects keypoints from the object’s model, and train a CNN to predict the vertex from every pixel to those keypoints. Besides keypoints, HybridPose [15] also employs edge vectors and symmetry correspondence to enrich the feature space for better estimation.

To further improve the estimation accuracy, another pipeline, RGBD-based methods additionally deploy depth information [4] [5] [16]. Early research [17] [18] compose contour vectors from RGB image and surface normal vectors from depth image, and estimate the pose by template matching. Recently, PVN3D [16] uses a neural network to separately extract image and point features, then encode them pointwisely to vote for 3D keypoints, and solve the pose with 3D-3D correspondence. REDE [6] also encode multimodal features, and applies an outlier elimination mechanism to train the network in an end-to-end manner. Because of the extra depth information, RGBD-based methods generally achieve better results than monocular-based methods.

B. Multi-view object pose estimation

The performance of single-view pose estimation methods are relevant to the quality of the query observation to a large extend. Occlusions, poor lighting conditions, and textureless object surfaces are all possible factors to affect the results. Hence, some researches involve more views of observations to estimate the pose [19] [20]. KeyPose [21] uses stereo images to generate depth maps and uplifts detected 2D keypoints to 3D space, so as to estimate the pose of textureless

transparent objects. [22] first estimates the pose in every single view as hypothesis, then votes for the hypothesis by measuring their relative discrepancy. Moreover, CosyPose [23] establish the consistency of objects across different views, then refine the pose with consistency and relative camera pose together. However, CosyPose still takes the pose estimated from every single view, and applies refinement in a backend manner. Our method differs from it in estimating the pose from both the query view and reference view in a frontend manner.

III. METHOD

In this section, we introduce our overall pipeline, as illustrated in Fig. 2. Taking the input reference image and query image, we extract 2D image features with a multi-scale feature extractor network. Then, we build a 3D geometric volume to learn the feature distribution in the 3D world space. By regularizing the distribution, we localize the 3D keypoints. Last, we adopt a soft RANSAC solver to solve the pose by 3D-3D correspondence. The whole process is iterated in a coarse-to-fine framework.

A. Multi-layer Feature Extraction

Given two input images of size $W \times H$, we use I_r to denote the reference image and I_q to denote the query image. Before applying keypoint prediction and pose estimation, we need to extract pixel-wise features from the input images. Since feature extraction is not the focus of this paper, we follow [14] to build a multi-scale convolutional neural network, to extract features at multiple resolutions. Because precise keypoint prediction requires both high-level semantic features and low-level context features, we adopt the output of the last upsampling layer of size $W \times H$, together with the output of the third from the last upsampling layer of size $W/4 \times H/4$, to build our 3D geometric volume. Also, to force the network to focus on the object rather than the

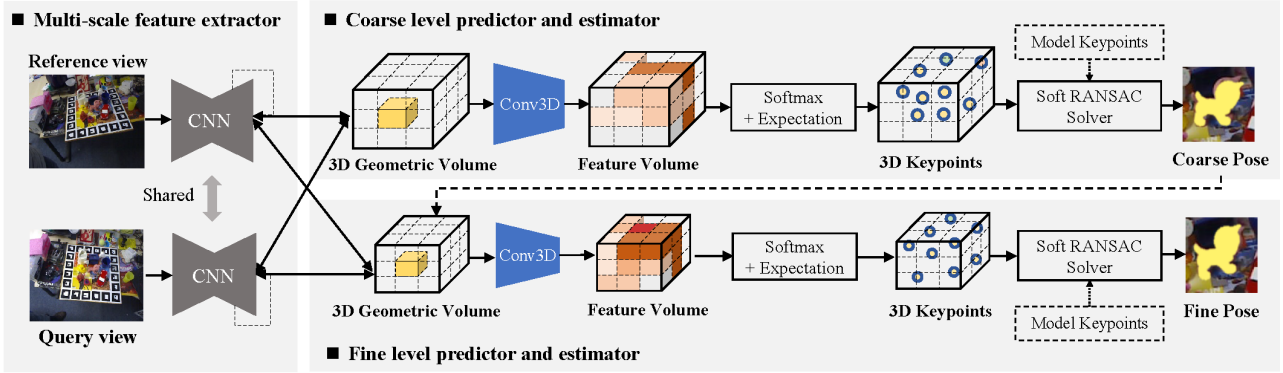


Fig. 2. **Method Overview.** Given two RGB images from reference view and query view, two feature maps are extracted by a multi-scale convolutional neural network. Then a 3D geometric volume is built surrounding an initial pose guess, which is then served to a 3D convolutional network to learn the feature distribution volume. The feature volume is then regularized to get the expected maximal value to predict 3D keypoints. Last, a soft RANSAC solver is deployed to solve the pose. The whole framework is conducted in a coarse-to-fine manner. The components covered in blue need to be trained.

whole scene, we take the output of the segmentation branch of the extractor as our predicted mask, and use these two masks to build the volume, too.

B. Constructing 3D Geometric Volume

To learn the 3D keypoint distribution, we directly build a 3D geometric volume in the 3D space. Without loss of generality, we divided the interested 3D space into regular 3D grids of size (H_v, W_v, D_v) , and the size of each grid is (h_v, w_v, d_v) . The axes of the grid coordinates are centralized in an initial guess and parallel to the reference camera coordinates.

With known camera intrinsic parameters $\{f_x, f_y, c_x, c_y\}$, we create a many to one projection from 3D grid space to image space by camera projection function $\pi(\cdot)$

$$z \begin{pmatrix} u \\ v \\ 1 \end{pmatrix} = \begin{pmatrix} f_x & 0 & c_x \\ 0 & f_y & c_y \\ 0 & 0 & 1 \end{pmatrix} \begin{pmatrix} x \\ y \\ z \end{pmatrix} \quad (1)$$

where (x, y, z) is point in 3D grid space, and (u, v) refers to image pixel position. The grid space is also projected to the query image space by the relative camera pose between the two views. This projection is fully differentiable, so it's feasible to be included as part of our network. It can be implemented by bilinear interpolation.

Through this process, each grid in 3D space is related to a point in the image space. Then we assign the high-level and low-level features extracted before of the 2D point to its related 3D point. In this way, we uplift the 2D features to the 3D space without approximation. Points projected outside the image are assigned to initial feature values.

What's more, considering that not only the features themselves, but also the relationship between two feature vectors of the same 3D point, comprise significant details of the object, we simply concatenate these two feature vectors, to keep as much information as possible for the following network to learn.

C. Coarse-to-fine Keypoint Prediction

Instead of regressing the geometric volume to get the 3D keypoints, we propose to learn the distribution of keypoints by reducing the divergence between the feature field and the local keypoint heatmaps. The local keypoint heatmaps are defined as

$$Q_i^k(p|m_i, \theta) \sim \mathcal{N}(\theta m_i, \sigma_i) \quad (2)$$

where $\{m_i\}_{i=1}^N$ refers to the model keypoints, θ is the target pose, and σ_i is the hyperparameters. This distribution represents the local heatmap we expect to be highlighted as possible keypoints locations.

And the feature field is defined as

$$Q_i^v(p|V(\cdot)) = \sum_{j \in \Omega} w_j V([p_j]) \quad (3)$$

where $\{w_j\}_{j \in \Omega}$ are the trilinear interpolation coefficients, $[p_j]$ are the 8 neighbour grids of the conditioned position p , and $V(\cdot)$ is the value operation in the feature field. This distribution describes how likely a position in the field is to be the keypoints.

To minimal the divergence of these two distribution, we adopt a Kullback-Leibler divergence loss as

$$Loss_{KL} = D_{KL}(Q^v \| Q^k) = - \sum_{i=1}^N Q_i^v \log\left(\frac{Q_i^k}{Q_i^v}\right) \quad (4)$$

To help the feature volume to learn the divergence, we build a simple 3-layers 3D convolutional neural network to intensify the difference, and add a softmax layer to regularize the output volume to further concentrate the distribution. After this process, the feature field is supposed to embody the distribution possibility of the expected keypoints. Hence, we maximize the marginal possibility of each dimension to find the optimal keypoint locations, and employ a smooth L_1 loss to evaluate the keypoints

$$Loss_{kpt} = \frac{1}{N} \sum_i^N smooth_{L_1}(p_i, \hat{p}_i) \quad (5)$$

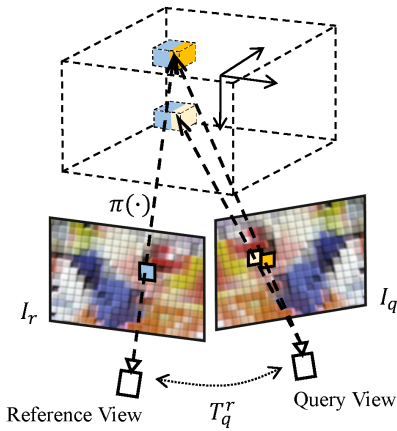


Fig. 3. **3D Geometric Volume.** A 3D geometric volume is constructed upon two feature maps. The 3D space is divided into regular grids. By camera projection matrix, each grid is projected back to 2D image space to get its related pixel. The two feature vectors of the two related pixels are concatenated together as the 3D grid’s feature.

It’s reasonable to assume that finer grid resolutions bring better prediction results. But higher resolution also costs more computation resources. Therefore, we employ a coarse-to-fine strategy. At the first coarse level, we build the 3D geometric volume with a resolution of $1cm$ and a larger space range. While at the second finer level, we decrease the size of each grid to $0.5cm$ and reduce the space range.

D. Soft Robust Solver

Given the predicted 3D keypoints $\{\hat{p}_i\}_{i=1}^N$ and the model keypoints $\{m_i\}_{i=1}^N$, we then solve the object pose by minimizing the distance between predicted points and model points. The optimization problem is

$$\hat{\theta} = \arg \min_{\theta} \|\theta m_i - \hat{p}_i\|_2 \quad (6)$$

where θ represents the 6D object pose.

Though this optimization problem can be solved by SVD in closed form, it is easy to be disturbed by outliers. Many recent works adopt RANSAC (RANDOM SAMPLE CONSENSUS) algorithm [24] or its variants to pick inliers [14] [16]. However, in our case, we only have N 3D points for optimization, the extra information needed to perform RANSAC is absent. Thus, directly applying the classic RANSAC algorithm is barely useful. Another reasonable approach is to apply a non-linear optimization solver to update the pose in the feature field, such as Gauss-Newton algorithm [25] or Levenberg-Marquardt algorithm [26]. But we find that the results are not as good as expected, probably because the distribution of the feature field is not convex everywhere, which leads to an incorrect updating orientation or excessive step. Therefore, we propose a soft RANSAC solver to softly count the inliers to solve a more robust pose.

Taken the predicted keypoints $\{\hat{p}_i\}_{i=1}^N$, we calculate all possible poses with every 3 points by SVD, which brings us a set of pose hypothesis $\{\theta_k\}_{k=1}^{C_N^3}$. For each hypothesis, we evaluate the distance for every predicted and model keypoints

under the hypothesis pose

$$d_{k,i} = \|\theta_k m_i - \hat{p}_i\|_2 \quad (7)$$

Then, instead of masking out the inliers with a hard threshold, we employ a sigmoid operation to softly classify the keypoints, and sum up the outputs of sigmoid as the soft inlier count of this hypothesis

$$Score_k = \sum_i^N \text{sigmoid}(\gamma_1(-d_{k,i} + \gamma_2)) \quad (8)$$

Last, we regularize the scores for all hypothesis by softmax, and softly aggregate them into a final pose

$$\hat{\theta} = \sum_k^K Score_k \cdot \theta_k \quad (9)$$

The loss to evaluate the predicted pose is

$$Loss_{pose} = \|\hat{t} - t\|_2 + \alpha \|\hat{R}R^T - I\|_F \quad (10)$$

In total, our network is trained with joint loss from both coarse level and fine level

$$Loss = \sum_j \beta_1 Loss_{pose_j} + \beta_2 Loss_{kpt_j} + \beta_3 Loss_{KL_j} \quad (11)$$

IV. EXPERIMENTS

In this section, we evaluate the proposed method by comparing it with the state-of-the-art methods on the Occlusion LineMOD dataset [27], to validate our strength in tackling occluded scenes using only RGB inputs.

A. Dataset

Occlusion LineMOD [27] dataset is a widely used benchmark for object 6D pose estimation task with serious occlusion. It contains 8 objects from the LineMOD dataset [18], but includes more challenges such as low resolution, cluttered scenes, and severe occlusions. In a lot of scenes of Occlusion LineMOD, only a small part of the object can be observed. Therefore, it’s a suitable dataset to evaluate our method. All the data is used for testing. The model is trained on LineMOD dataset. During training and testing, we pair up every two adjacent frames in the test list. The average relative camera distance of all the testing pairs is $0.168m$, and the minimal distance is $0.004m$.

B. Metrics

In object pose estimation task, the most commonly used metrics are ADD [17] and ADD-S [1]. Given an object model of M points, ADD metric evaluates the average distance between model points transformed with predicted and ground truth pose respectively

$$ADD = \frac{1}{M} \sum_{i=1}^M \|\theta p_i - \hat{\theta} p_i\|_2 \quad (12)$$

While ADD-S metric calculates the average distance between the closest points, which is used for evaluating symmetric object

$$ADD-S = \frac{1}{M} \sum_{i=1}^M \min_{j \in M} \|\theta p_j - \hat{\theta} p_i\|_2 \quad (13)$$

We use ADD for non-symmetric objects and ADD-S for symmetric objects. An estimation is regarded successful if the ADD(-S) is less than 10% of the object’s diameter.

C. Implementation Details

In implementation, we follow [14] to select 9 keypoints for every object, and perform the same data augmentation.

In the coarse level, we compute the center pixel position in the predicted mask in reference view, and unproject it to a 3D position with a prior depth, which is the average of the object depths in the dataset. Then, we build the 3D geometric volume around this initial position in range $[-0.3, 0.3] \times [-0.3, 0.3] \times [-0.3, 0.3]$ (meters), with grid size of $0.01m$. The keypoint prediction network contains three 3D convolutional layers, each followed with a 3D BatchNorm layer and a ReLU layer, one output 3D convolutional layer, and finally a LogSoftmax layer.

In the fine level, we take the estimated position from the coarse level as the initial position, and build the 3D geometric volume around it with grid size of $0.005m$. The range of the fine volume is dependent on the diameter of each object. The keypoint prediction network is nearly the same as the network used in the coarse level, but contains one less convolutional layer.

We run all our training and experiments on a machine equipped with an Intel(R) Xeon(R) Silver 4216 CPU at 2.10GHz, and an NVIDIA GeForce RTX 3090 GPU.

TABLE I
PERFORMANCE COMPARISON ON OCCLUSION LINEMOD
(ADD(-S) < 0.1d).

	RGB		2-view RGB		
	PoseCNN [1]	PVNet [14]	Hu [28]	Late-fusion	Ours
ape	9.6	15.8	12.1	34.5	37.2
can	45.2	63.3	39.9	57.9	64.6
cat	0.93	16.7	8.2	24.3	22.8
driller	41.4	65.7	47.1	58.3	67.2
duck	19.6	25.2	11.0	33.5	36.9
eggbox*	22.0	50.2	24.7	46.3	42.3
glue*	38.5	49.6	39.5	60.0	62.2
holepuncher	22.1	39.7	21.9	41.6	43.7
average	24.9	40.8	27.0	44.6	47.1

*denotes symmetric objects.

D. Results on Benchmark Dataset

We evaluate the performance of our method in Occlusion LineMOD dataset, to compare with state-of-the-art monocular-based methods and the other 2-view method late-fusion, as shown in Table. I. Since the late-fusion approach

TABLE II
COMPARISON OF AVERAGE 3D KEYPOINT PREDICTION ERROR.

	Late-fusion	REDE [6]	Ours
ape	0.121	0.030	0.043
can	0.048	0.034	0.032
cat	0.261	0.090	0.114
driller	0.065	0.041	0.029
duck	0.176	0.034	0.035
holepuncher	0.084	0.058	0.027
average	0.126	0.048	0.047

hasn’t been explored by other works to our best knowledge, we implement the approach by ourselves. For fair comparison, we take the 2D predicted keypoints from PVNet [14], and triangulate the two keypoints to 3D space by classic method [29]. By doing so, the late-fusion approach shares the same feature maps with our proposed method, and the major difference lies in the keypoint prediction mechanism.

Pose estimation under serious occlusion situations is a difficult task, especially for monocular-based methods, thus not a lot of current methods report their performance in this dataset. As the table shows, 2-view based methods generally acquire better results than the monocular-based methods, illustrating the benefits of introducing stereopsis in the estimation task. Compared to the other 2-view method late-fusion, our method exceeds with a margin of 3.5%, which indicates the advantage of early geometric fusion of 2D features. Overall, our method achieves the best performance in 6 classes and gets the highest average recall.

To verify our robustness towards occlusion, we also draw accuracy curve under increasing levels of invisible surfaces on Occlusion LineMOD dataset. Following [4], levels of occlusion are measured by calculating the invisible surface percentage of model points projected in the image frame. We measure the performance in the whole Occlusion LineMOD dataset. The accuracy of ADD(-S) smaller than $0.1d$ curve is shown in Fig. 4, it can be seen that our performance under occlusion is more stable compared to monocular-based methods and the late-fusion approach, especially in heavy occlusion situations.

What’s more, we present the average 3D keypoint prediction L2 error in Table. II. The error is calculated between our predicted scene 3D keypoints and ground truth scene keypoints with an L2 distance. We compare the distance with the late-fusion approach and a RGBD-based method [6]. Except for symmetric objects, our method predicts 3D keypoints with a slightly better accuracy than the RGBD-based methods [6], and far better than the late-fusion approach with a margin of $0.079m$.

Some visualization results are shown in Fig. 5. We project the object CAD model transformed by the estimated pose and draw the points on the reference view. All the images are cropped for better visualization, and the query view is cropped with the same position and size to show the parallax. It can be observed that compared with [14] and late-fusion approach, our method can accurately estimate the pose of

objects, especially in some hard cases with occlusion.

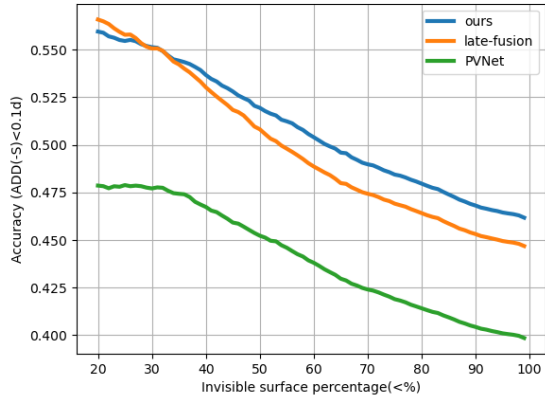


Fig. 4. Performance with respect to invisible surface percentage. Invisible surface percentage is computed as the ratio between invisible mask area whole mask area. The proposed method is more robust under heavy occlusion situation.

TABLE III
ABLATION STUDY ON COARSE-TO-FINE MECHANISM.

	coarse		coarse+fine	
	ADD(-S) (avg/med)	<0.1d	ADD(-S) (avg/med)	<0.1d
ape	0.045/0.017	29.3	↓ 0.005/0.003	↑ 7.9
can	0.032/0.017	55.9	↓ 0.005/0.003	↑ 8.7
cat	0.128/0.096	15.3	↓ 0.026/0.039	↑ 7.5
driller	0.032/0.020	61.4	↓ 0.004/0.002	↑ 5.8
duck	0.040/0.019	28.9	↓ 0.005/0.003	↑ 8.0
eggbox*	0.096/0.037	32.7	↓ 0.015/0.015	↑ 9.6
glue*	0.066/0.014	55.9	↓ 0.004/0.003	↑ 6.3
holepuncher	0.030/0.018	39.4	↓ 0.003/0.002	↑ 4.3
average		39.9		↑ 7.2

*denotes symmetric objects.

E. Ablation Study

To validate the proposed coarse-to-fine mechanism, we compare the results after only coarse level network to the final coarse-to-fine network. The experiments are conducted in Occlusion LineMOD dataset. Table. III summarize the results. With the help of the coarse-to-fine mechanism, the recall of every class is increased with an average improvement of 7.2%. Also, the average and medium ADD are all decreased, especially in hard classes such as cat and eggbox, with reductions of 0.026/0.039 and 0.015/0.015 respectively. The results verify the benefits of learning the keypoint distribution from coarse resolution to finer resolution, and the ability of the mechanism to improve an incorrect initial guess to a certain extent.

V. CONCLUSIONS

In this paper, we propose an geometric volume fusion based object 6D pose estimation method under short-baseline two-view setting. We build a geometric volume in 3D space

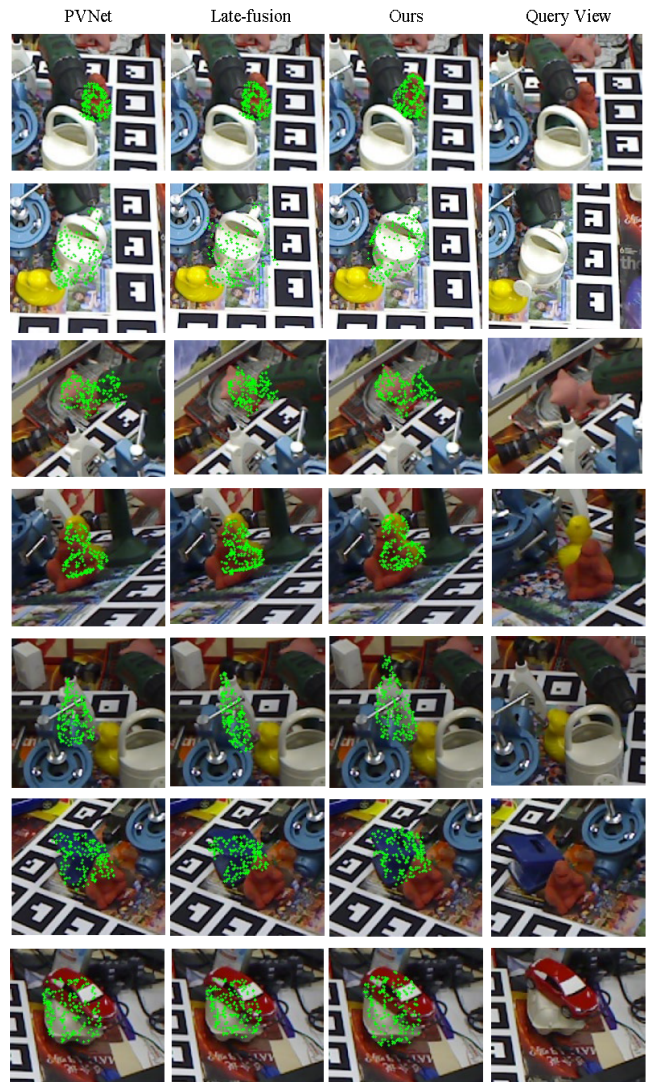


Fig. 5. **Visualization Results Samples.** Some visualization results on OCC-LM dataset. All the points are projected to the reference image by estimated pose of different methods. The last column shows the query view used in our proposed method. All images are cropped for better visualization, and the query view is cropped with the same position and size as the reference view to show the parallax. The last row shows a failure case in eggbox class.

to restore the object’s 3D information from two monocular RGB images. By regularization and learning, the volume is trained to highlight the position of object keypoints. A soft ransac solver is deployed to solve the pose in closed form. In addition, we deploy a coarse-to-fine framework to improve the estimation accuracy. Experiments show that our method outperforms the state-of-the-art monocular-based methods and our baselines in serious occlusion datasets.

REFERENCES

- [1] Y. Xiang, T. Schmidt, V. Narayanan, and D. Fox, “Posecnn: A convolutional neural network for 6d object pose estimation in cluttered scenes,” *arXiv preprint arXiv:1711.00199*, 2017.
- [2] K. Park, T. Patten, and M. Vincze, “Pix2pose: Pixel-wise coordinate regression of objects for 6d pose estimation,” in *Proceedings of the*

- IEEE/CVF International Conference on Computer Vision*, pp. 7668–7677, 2019.
- [3] Y. Li, G. Wang, X. Ji, Y. Xiang, and D. Fox, “Deepim: Deep iterative matching for 6d pose estimation,” in *Proceedings of the European Conference on Computer Vision (ECCV)*, pp. 683–698, 2018.
 - [4] C. Wang, D. Xu, Y. Zhu, R. Martín-Martín, C. Lu, L. Fei-Fei, and S. Savarese, “Densefusion: 6d object pose estimation by iterative dense fusion,” in *Proceedings of the IEEE/CVF conference on computer vision and pattern recognition*, pp. 3343–3352, 2019.
 - [5] K. Wada, E. Sucar, S. James, D. Lenton, and A. J. Davison, “Morefusion: Multi-object reasoning for 6d pose estimation from volumetric fusion,” in *Proceedings of the IEEE/CVF conference on computer vision and pattern recognition*, pp. 14540–14549, 2020.
 - [6] W. Hua, Z. Zhou, J. Wu, H. Huang, Y. Wang, and R. Xiong, “Rede: End-to-end object 6d pose robust estimation using differentiable outliers elimination,” *IEEE Robotics and Automation Letters*, vol. 6, no. 2, pp. 2886–2893, 2021.
 - [7] J.-R. Chang and Y.-S. Chen, “Pyramid stereo matching network,” in *Proceedings of the IEEE Conference on Computer Vision and Pattern Recognition*, pp. 5410–5418, 2018.
 - [8] P. Li, X. Chen, and S. Shen, “Stereo r-cnn based 3d object detection for autonomous driving,” in *Proceedings of the IEEE/CVF Conference on Computer Vision and Pattern Recognition*, pp. 7644–7652, 2019.
 - [9] Y. Yao, Z. Luo, S. Li, T. Fang, and L. Quan, “Mvsnet: Depth inference for unstructured multi-view stereo,” in *Proceedings of the European Conference on Computer Vision (ECCV)*, pp. 767–783, 2018.
 - [10] M. Rad and V. Lepetit, “Bb8: A scalable, accurate, robust to partial occlusion method for predicting the 3d poses of challenging objects without using depth,” in *Proceedings of the IEEE International Conference on Computer Vision*, pp. 3828–3836, 2017.
 - [11] S. Zakharov, I. Shugurov, and S. Ilic, “Dpod: 6d pose object detector and refiner,” in *Proceedings of the IEEE/CVF International Conference on Computer Vision*, pp. 1941–1950, 2019.
 - [12] B. Tekin, S. N. Sinha, and P. Fua, “Real-time seamless single shot 6d object pose prediction,” in *Proceedings of the IEEE Conference on Computer Vision and Pattern Recognition*, pp. 292–301, 2018.
 - [13] Q. Luo, H. Ma, L. Tang, Y. Wang, and R. Xiong, “3d-ssd: Learning hierarchical features from rgb-d images for amodal 3d object detection,” *Neurocomputing*, vol. 378, pp. 364–374, 2020.
 - [14] S. Peng, Y. Liu, Q. Huang, X. Zhou, and H. Bao, “Pvnet: Pixel-wise voting network for 6dof pose estimation,” in *Proceedings of the IEEE/CVF Conference on Computer Vision and Pattern Recognition*, pp. 4561–4570, 2019.
 - [15] C. Song, J. Song, and Q. Huang, “Hybridpose: 6d object pose estimation under hybrid representations,” in *Proceedings of the IEEE/CVF conference on computer vision and pattern recognition*, pp. 431–440, 2020.
 - [16] Y. He, W. Sun, H. Huang, J. Liu, H. Fan, and J. Sun, “Pvn3d: A deep point-wise 3d keypoints voting network for 6dof pose estimation,” in *Proceedings of the IEEE/CVF conference on computer vision and pattern recognition*, pp. 11632–11641, 2020.
 - [17] S. Hinterstoisser, V. Lepetit, S. Ilic, S. Holzer, G. Bradski, K. Konolige, and N. Navab, “Model based training, detection and pose estimation of texture-less 3d objects in heavily cluttered scenes,” in *Asian conference on computer vision*, pp. 548–562, Springer, 2012.
 - [18] S. Hinterstoisser, S. Holzer, C. Cagniart, S. Ilic, K. Konolige, N. Navab, and V. Lepetit, “Multimodal templates for real-time detection of texture-less objects in heavily cluttered scenes,” in *2011 international conference on computer vision*, pp. 858–865, IEEE, 2011.
 - [19] A. Collet and S. S. Srinivasa, “Efficient multi-view object recognition and full pose estimation,” in *2010 IEEE International Conference on Robotics and Automation*, pp. 2050–2055, IEEE, 2010.
 - [20] A. Collet, M. Martinez, and S. S. Srinivasa, “The moped framework: Object recognition and pose estimation for manipulation,” *The international journal of robotics research*, vol. 30, no. 10, pp. 1284–1306, 2011.
 - [21] X. Liu, R. Jonschkowski, A. Angelova, and K. Konolige, “Keypose: Multi-view 3d labeling and keypoint estimation for transparent objects,” in *Proceedings of the IEEE/CVF conference on computer vision and pattern recognition*, pp. 11602–11610, 2020.
 - [22] C. Li, J. Bai, and G. D. Hager, “A unified framework for multi-view multi-class object pose estimation,” in *Proceedings of the european conference on computer vision (eccv)*, pp. 254–269, 2018.
 - [23] Y. Labbé, J. Carpentier, M. Aubry, and J. Sivic, “Cosypose: Consistent multi-view multi-object 6d pose estimation,” in *European Conference on Computer Vision*, pp. 574–591, Springer, 2020.
 - [24] M. A. Fischler and R. C. Bolles, “Random sample consensus: a paradigm for model fitting with applications to image analysis and automated cartography,” *Communications of the ACM*, vol. 24, no. 6, pp. 381–395, 1981.
 - [25] H. O. Hartley, “The modified gauss-newton method for the fitting of non-linear regression functions by least squares,” *Technometrics*, vol. 3, no. 2, pp. 269–280, 1961.
 - [26] J. J. Moré, “The levenberg-marquardt algorithm: implementation and theory,” in *Numerical analysis*, pp. 105–116, Springer, 1978.
 - [27] E. Brachmann, A. Krull, F. Michel, S. Gumhold, J. Shotton, and C. Rother, “Learning 6d object pose estimation using 3d object coordinates,” in *European conference on computer vision*, pp. 536–551, Springer, 2014.
 - [28] Y. Hu, J. Hugonot, P. Fua, and M. Salzmann, “Segmentation-driven 6d object pose estimation,” in *Proceedings of the IEEE/CVF Conference on Computer Vision and Pattern Recognition*, pp. 3385–3394, 2019.
 - [29] G. Bradski, “The opencv library,” *Dr. Dobbs’s Journal: Software Tools for the Professional Programmer*, vol. 25, no. 11, pp. 120–123, 2000.